Predictive modeling of hematoma expansion from non-contrast computed tomography in spontaneous intracerebral hemorrhage patients

Natasha Ironside, MBChB[1]; Kareem El Naamani, MD[2]; Tanvir Rizvi, MD[3]; Mohammed Shifat E-Rabbi, PhD[4]; Shinjini Kundu, MD, PhD[5]; Andrea Becceril-Gaitan, MD[6]; Kristofor Pas, BS[4]; Harrison Snyder, MD[6], Ching-Jen Chen, MD[7]; Carl D. Langefeld, PhD[8], Daniel Woo, MD[9]; Stephan Mayer, MD[10]; E. Sander Connolly, MD[11]; Gustavo Rohde, PhD[4,12] on behalf of the ERICH Investigators and the VISTA-ICH collaboration*

[1]*Department of Neurological Surgery, University of Virginia Health System, Charlottesville, VA*
[2]*Department of Neurological Surgery, Thomas Jefferson University, Philadelphia, PA*
[3]*Department of Radiology, University of Virginia Health System, Charlottesville, VA*
[4]*Department of Biomedical Engineering, University of Virginia, Charlottesville, VA*
[5]*Department of Radiology, Washington University in St. Louis, St. Louis, MO*
[6]*Department of Neurological Surgery, Tufts University Medical Center, Boston, MA*
[7]*Department of Neurosurgery, The University of Texas Health Science Center, Houston, TX*
[8]*Department of Biostatistics and Data Science, Wake Forest University School of Medicine, Winston-Salem, NC*
[9]*Department of Neurology, University of Cincinnati, Cincinnati, Ohio*
[10]*Department of Neurology, Westchester Medical Center, Westchester, NY*
[11] *Department of Neurological Surgery, Vagelos College of Physicians and Surgeons, Columbia University, New York, NY*
[12] *Department of Electrical and Computer Engineering, University of Virginia, Charlottesville, VA*

***VISTA-ICH Steering Committee:** DF Hanley (Chair), K Butcher, S Davis, B Gregson, KR Lees, P Lyden, S Mayer, K Muir, and T Steiner

Running title: Hematoma expansion prediction after ICH

Key words: intracerebral hemorrhage; hematoma expansion; artificial intelligence; automated prediction; transport-based morphometry; computed tomography; machine learning

Figures/Tables: Figures: 5, Tables : 1

Acknowledgements: We wish to acknowledge Eric Oermann, MD, PhD for generously reading the draft manuscript.

Correspondance:
Natasha Ironside, MBChB
Department of Neurological Surgery
University of Virginia Health System
1215 Lee Street
Charlottesville
Virginia 22903

USA
+14349240000
ni8vb@uvahealth.org

Abstract

Hematoma expansion is a consistent predictor of poor neurological outcome and mortality after spontaneous intracerebral hemorrhage (ICH). An incomplete understanding of its biophysiology has limited early preventative intervention. Transport-based morphometry (TBM) is a mathematical modeling technique that uses a physically meaningful metric to quantify and visualize discriminating image features that are not readily perceptible to the human eye. We hypothesized that TBM could discover relationships between hematoma morphology on initial Non-Contrast Computed Tomography (NCCT) and hematoma expansion. 170 spontaneous ICH patients enrolled in the multi-center international Virtual International Trials of Stroke Archive (VISTA-ICH) with time-series NCCT data were used for model derivation. Its performance was assessed on a test dataset of 170 patients from the Ethnic/Racial Variations of Intracerebral Hemorrhage (ERICH) study. A unique transport-based representation was produced from each presentation NCCT hematoma image to identify morphological features of expansion. The principal hematoma features identified by TBM were larger size, density heterogeneity, shape irregularity and peripheral density distribution. These were consistent with clinician-identified features of hematoma expansion, corroborating the hypothesis that morphological characteristics of the hematoma promote future growth. Incorporating these traits into a v achieved a AUROC of 0.71 for quantifying 24-hour hematoma expansion risk in the test dataset. This outperformed existing clinician protocols and alternate machine learning methods, suggesting that TBM detected features with improved precision than by visual inspection alone. This pre-clinical study presents a quantitative and interpretable method for discovery and visualization of NCCT biomarkers of hematoma expansion in ICH patients. Because TBM has a direct physical meaning, its modeling of NCCT hematoma features can inform hypotheses for

hematoma expansion mechanisms. It has potential future application as a clinical risk stratification tool.

Introduction

Within hours of spontaneous intracerebral hemorrhage (ICH) onset, hematoma expansion contributes to mass effect and injury to the surrounding brain.[1-3] It is a preventable predictor of poor neurological outcome and mortality.[1,2] Biophysical hypotheses for hematoma expansion are primarily derived from small pathological studies and have not been proven in the clinical setting.[1,2] Although several non-contrast computed tomography (NCCT) features for hematoma expansion have been independently described by clinicians (i.e. swirl sign, blend sign, island sign), a quantitative method for analyzing hematoma morphology from NCCT is lacking.[7-10] Recent results demonstrating the benefit to ICH surgical evacuation motivates new approaches to enable early detection of hematoma expansion and reduce time-to-intervention in future ICH trial designs.[4-6] Understanding the relationship between NCCT changes in hematoma morphology and the underlying expansion mechanism will be crucial to identifying preventative therapies.[3-5]

Qualitative NCCT markers of hematoma expansion named by clinicians have been incorporated into clinical scoring systems to predict hematoma expansion. However, their use of subjective criteria has led to scoring variability.[2,5,8-10] Furthermore, use of different terminologies to describe similar features has limited our understanding of the relative diagnostic value of each feature.[2,5,8-10] Deep learning methods for NCCT radiographic marker identification carry advantages of being entirely data-driven and automated.[6] However, they are also limited by their

lack of interpretability and provide little to no consideration of the biophysical processes necessary to provide a scientific rationale for their use.[12,13] There exists a clear need for development of a quantitative and interpretable methodology for NCCT radiographic marker identification which could improve our understanding of hematoma expansion.

Transport-based morphometry (TBM) is a quantitative modeling technique that generates a three-dimensional representation of the entire information content within an image.[7,8] TBM subsumes well-established image features used in protocols, while also considering features not readily discernible to the human eye.[7] Model inversion permits visualization of discriminating morphological and spatial information.[9] In this pre-clinical study of segmented time-series NCCT hematoma images, we hypothesized that transport-based morphometry (TBM) could discover relationships between NCCT morphometric features and hematoma expansion. [17-20] Data from the ICH section of the multicenter Virtual International Trials in Stroke Archive (VISTA-ICH) was used to derive the model, and the Ethnic/Racial Variations of Intracerebral Hemorrhage (ERICH) study was used for external validation.[14-16] We demonstrate that (1) TBM model regression can quantify changes in NCCT hematoma morphology to estimate risk of expansion, (2) TBM model inversion permits visualization of NCCT features of expansion to inform hypotheses for its biophysical mechanisms, and (3) a resulting predictive model for future expansion can outperform conventional clinician protocols and machine learning methods.

Results

Dataset composition

Of the 265 spontaneous ICH patients in the VISTA repository with available presentation NCCT scans, 95 were excluded (26 for corrupted/unreadable DICOM files, 3 for surgical evacuation, 9 for infratentorial location, 3 for no 24±6 hour interval NCCT scan and 52 for initial ICH volume <7mL). The remaining 170 patients (mean (SD) age 64.08 (12.45) years; 37.6% (n=64) female), comprised the derivation (training and internal validation) dataset. In the derivation dataset, the mean (SD) and median [IQR] hematoma volumes at presentation were 31.31 (24.06) and 25 [14-39] mL, respectively. The mean (SD) and median [IQR] hematoma volumes at 24±6 hours were 39.56 (34.42) and 28 [14-54] mL, respectively. Hematoma expansion was present in 32.9% (n=56) patients. Of the 3,000 spontaneous ICH patients in the ERICH study, 1,066 met inclusion criteria and were randomly sampled to generate a test (external validation) dataset of 170 patients, (mean (SD) age 61.14 (13.38) years; 29.2% (n=50) female), 20.0% (n=34) Black, 42.9% (n=73) Hispanic and 35.3% (n=60) White. In the test dataset, the mean (SD) and median [IQR] hematoma volumes at presentation were 25.73 (19.73) and 21 [11-33] mL, respectively. The mean (SD) and median [IQR] hematoma volumes at 24±6 hours were 31.59 (24.24) and 26 [12-43] mL, respectively. Hematoma expansion was present in 32.9% (n=56) patients. A flow diagram of the patient selection process for the derivation and test datasets is shown in **eFigure 1**. Comparisons of baseline demographic and clinical characteristics between the expansion and no expansion groups for each of the derivation and test datasets are presented in **Table1**.

Data preprocessing

The NCCT preprocessing and segmentation results are shown in **Figure 1A-I**. Comparisons of the native NCCT segmented hematoma images did not reveal a visually discernible difference between the expansion (**Figure 1J)** and no expansion groups (**Figure 1K)**. The intrinsic mean template $I_{0\mu}$ used for the optimization of the linear optimal transportation framework is shown

for the original and location-adjusted datasets in **eFigure 2**.

TBM model regression quantified 24-hour hematoma growth from NCCT

In the internal validation cohort of the derivation dataset, the mean correlation co-efficient (CC) for the most correlated direction in transport space, w_{corr}, between presentation hematoma features and 24-hour absolute hematoma volume increase was 0.191 [0.184-0.198], p<0.0001 for TBM alone. This improved to 0.278 [0.271–0.285]; p<0.0001 after location and clinical information were included in the TBM model **(eFigure 7)**. Stepwise optimization results for the preliminary hematoma growth prediction models are presented in the **Online-only supplement; eFigures 7 and 8.** When assessed in the test dataset, the final TBM model adjusted for location and clinical information quantified 24-hour volume increase from presentation hematoma features with a CC of 0.245; p=0.002 **(Figure 3A)**.

TBM predicted 24-hour hematoma expansion from NCCT

In the internal validation cohort of the derivation dataset, there was a separation of the mean probability distributions for the expansion and no expansion groups when projected onto the most discriminant direction in transport space w^0 (p<0.0001) **(eFigure 3A-D)**. The classifier trained on w^0 predicted expansion with a mean area under the receiver operating curve (AUROC) of 0.643 [0.640-0.648] for TBM alone. This improved to 0.698 [0.695-0.702] when location and clinical information were included in the TBM model **(eFigure 4A and 4D)**. The mean accuracy, sensitivity and specificity were 67.9% [67.6-68.2%], 51.0% [50.5-51.6%], and 77.6% [77.3-77.9%], respectively for the clinical information and location-adjusted TBM model. Stepwise optimization results for the preliminary expansion prediction models are presented in the **Online-**

only supplement; eFigures 3, 4, 5, 6.

When assessed in the test dataset, the final clinical information and location-adjusted TBM model achieved a significant separation between the mean probability distributions for the expansion and no expansion groups when projected onto w^0 ($p<0.0001$) **(Figure 2A).** This corresponded to an AUROC of 0.705 for discriminating expansion from no expansion (**Figure 2B**). In the test dataset, the accuracy, sensitivity and specificity were 70.0%, 73.7% and 63.8%, respectively.

TBM discovers interpretable NCCT features of 24-hour hematoma expansion and growth

In contrast to the native NCCT segmented hematoma images, TBM-generated images discovered a visually discernible difference between the expansion and no expansion groups. The inverse transformations of the hematoma features projected onto w^0 are shown in **Figures 2C and 2D**, plotted in units of standard deviations (SD) of the pixel intensity distribution along w^0. The visible features that discriminated expansion were larger size, elongated shape, peripheral density distribution, and density heterogeneity.

TBM-generated images also discovered a visually discernible change in NCCT features correlating with increasing 24-hour hematoma growth. The inverse transformations of the presentation hematoma features projected onto w_{corr} are shown in **Figure 3B and 3C**, plotted in units of SD of the pixel intensity distribution along w_{corr}. The features associated with more growth were larger size, peripheral density distribution and density heterogeneity.

To objectively assess the significance of the TBM-generated NCCT features of hematoma expansion, we measured each feature from the native NCCT images. Hematoma size ($p<0.0001$), density heterogeneity ($p<0.0001$), elongated shape ($p<0.0001$) and peripheral density distribution ($p<0.0001$) demonstrated separation of the mean probability distributions between the expansion and no expansion groups in the derivation dataset **(eFigures 10 and 11)**.

We then assessed the predictive performance of each TBM-identified NCCT hematoma feature of expansion from the native NCCT images. The AUROC for predicting 24-hour hematoma expansion was 0.577 for hematoma size, 0.578 for density heterogeneity, 0.529 for elongated shape, and 0.560 for peripheral density distribution in the test dataset. AUROC curves for predicting 24-hour hematoma expansion from the TBM-identified NCCT image features in the derivation and test datasets are presented in **eFigure 12.** The clinical information and location-adjusted TBM model outperformed each image feature in predicting 24-hour hematoma expansion in both the derivation and test datasets.

Hematoma location independently affects hematoma expansion

Because hematoma location information improved the performance of the TBM model, we assessed its independent effect on expansion. In the internal validation cohort of the derivation dataset, there was separation of the mean probability distributions of hematoma location between the expansion and no expansion groups when projected onto w^0 ($p<0.0001$) **(eFigure 9C).** The mean AUROC for hematoma location discriminating the expansion and no expansion groups was 0.600 [0.597-0.603] **(eFigure 9A).**

TBM-generated images discovered visibly discernible hematoma locations discriminating expansion. The inverse transformations plotted in unit vectors along w^0 in the axial, coronal and sagittal planes showed hematomas associated with greater likelihood of expansion to be oriented posteriorly, inferiorly and medially towards the thalamus, posterior limb of the internal capsule and the atrium of the lateral ventricle **(Figure 4)**.

TBM as an alternative to clinician-based hematoma expansion prediction scores

We assessed the predictive performance of established clinician-based hematoma expansion prediction scores in our datasets. The AUROC for predicting 24-hour hematoma expansion was 0.643 for BAT, 0.652 for BRAIN, 0.565 for HEAVN, 0.569 for HEP, and 0.602 for the 10-point score in the test dataset **(Figure 5)**. Comparisons between the TBM model and clinician-based scores for predicting 24-hour hematoma expansion and 24-hour hematoma growth in the derivation dataset are presented in **eFigures 13 and 14.** The clinical information and location-adjusted TBM model demonstrated improved performance over clinician-based scoring methods for predicting 24-hour hematoma expansion in both the derivation and test datasets.

TBM as an alternate to machine and deep learning methods for hematoma expansion prediction

Alternate machine and deep learning methods for hematoma expansion prediction were trained using the derivation dataset, and we assessed their predictive performance in the test dataset. The AUROC for predicting 24-hour hematoma expansion was 0.511 for K-nearest neighbors, 0.501 for support vector machine, 0.535 for logistic regression, and 0.557 for 3D ResNet convolutional neural networks in the test dataset **(eFigure 14)**. The clinical information and location-adjusted TBM model demonstrated improved performance over alternate machine learning and deep

learning methods for predicting 24-hour hematoma expansion in the test dataset.

Discussion

Hematoma expansion is a consistent predictor of poor neurological outcome and mortality after spontaneous ICH.[4,10-12] Although early detection of hematoma expansion is paramount to implementation of preventative therapies, knowledge of its underlying biophysiological processes is lacking.[2,13] This has impaired progress towards efficient and reliable methods for detecting patients at risk for expansion.[5] In this study, we developed a quantitative method for investigating NCCT hematoma morphology. Our TBM framework discovered hematoma morphological changes associated with expansion and was interpretable through model inversion. This novel approach discovers hypotheses for hematoma expansion pathophysiology and has the potential to improve its clinical prediction.

We considered normalized Hounsfield Unit (HU) pixel intensity values as relative measurements of blood density and applied our transport-based morphometry (TBM) technique to model the relative intensity of each pixel in a segmented NCCT hematoma image with reference to a template.[17-20] Thus, optimal transportation-based modeling of hematoma images provided insight into inherent physical phenomena.[9,14] When linear models were applied to the resulting transport space representations, we found a significant correlation between NCCT hematoma morphological changes and 24-hour hematoma growth. Inclusion of clinical variables and spatial location achieved further improved performance, resulting in an AUC of 0.71 for predicting hematoma expansion. Taken together, our findings suggest that TBM could discriminate 24-hour

hematoma expansion from NCCT image features.

One advantage of our method is its interpretability. Feature visualization by TBM provided radiographic insight into the process of hematoma expansion.[14] The conventional biological model for hematoma expansion is the “avalanche effect”, first observed in a pathological study from 1971.[2] This described the process of secondary mechanical shearing of neighboring vessels at the periphery of the hematoma, resulting in successive bleeding. It was corroborated by a more recent pathological study that observed hematomas to expand in the perivascular spaces and detach branches from surrounding tissue, resulting in secondary bleeding.[1] These proposed mechanisms of hematoma expansion have not previously been examined in a large real-time patient sample. When we inverted our TBM model to generate visualizations of the NCCT features correlating most with expansion, we discovered morphological characteristics of expansion that were not visibly discernible on the native images. Notably, we observed preferential distribution of density towards the periphery of the expanding hematoma, which may be consistent with involvement of secondary circumferential vessels. Density heterogeneity further suggested that the hematoma expanded from bleeding at different times and locations.

While the affected location may harbor characteristic structural properties that facilitate expansion, there is conflicting evidence regarding location(s) with the propensity for expansion.[15] Hematoma location has not yet been included as a potential modifier in expansion prediction scores.[5,12,16] We defined location from the center of the hematoma, finding it to be a significant independent predictor of expansion that improved the TBM model’s performance. The location most discriminating expansion was oriented towards the thalamus, posterior limb of the internal

capsule and atrium of the lateral ventricle. This correlated with the orientation of the perivascular spaces and the proposed pathological mechanism of blood product transit via these spaces, representing the path of least resistance surrounding the hematoma.[17] These findings lend weight to the importance of further study into the relationships between NCCT image characteristics and the biomechanics of hematoma expansion.

The shape, size and density NCCT characteristics identified by TBM are consistent with those previously described by clinicians.[18,19] This emphasizes similarities between our TBM model and clinician-based interpretation of ICH from NCCT, corroborating their hypothesis that morphological characteristics of the hematoma promote future growth.[5,18] In contrast to clinician-based methods, TBM overcame the subjectivity inherent to qualitative ranking, standardized the range of terminologies that have previously been attributed to similar image features, and permitted grading of severity. When we measured TBM-identified NCCT image features from the native image data, they were statistically significant predictors of expansion but each was outperformed by the final TBM model in the test dataset. Similarly, TBM outperformed established clinician-based NCCT prediction scores and emerging machine learning models.[16,20-23] By including all information contained within a segmented hematoma image, we propose that TBM achieved greater precision and improved generalizability than pre-specified feature detection alone.[24] Like RAPID-AI for ischemic stroke, further optimization of TBM could lead to a reliable and efficient method for hematoma expansion prediction to select patients for timely intervention.[25,26]

Several limitations to this study must be acknowledged. Although we included a representative

multi-national population of patients enrolled in ICH clinical trials with standardized time-series NCCT data, our model derivation cohort was limited by its small sample size of 170 patients and retrospective design.[27] Because we randomly sampled an equivalent-sized external validation dataset from the ERICH cohort study, the generalizability of the results are limited by the potential for confounding factors inherent to the validation dataset that were not accounted for. Future validation studies should investigate larger cohorts and/or matching paradigms to account for this limitation prior to drawing conclusions as to the potential clinical utility of TBM. The limited density information on NCCT and the small number of patients who experienced hematoma expansion in our dataset are likely to have affected the predictive strength of the model.[7,8,28] Therefore, in spite of dimensionality reduction and external validation, our model remains at risk of overfitting. Our AUC of 0.71 in the external validation dataset, while superior to alternate clinician-based and machine learning methods, indicates moderate predictive performance, and is not yet sufficient for clinical application. In addition, the poor performance of alternate machine learning methods in our test dataset warrants further investigation for potential sampling errors. Future external validation studies should consider case-matched patient sampling, adjustment for confounders, and consideration of multiple cross-validation resampling methods prior to defining an optimal model. The relative importance of demographic and clinical predictors of hematoma expansion and the methods for incorporating these data into predictive modeling also warrants further investigation in future studies. Because our expansion definition was not based on clinical outcome, we expect future studies to investigate relationships between NCCT hematoma morphology, hematoma expansion, and neurological outcome. The derivation dataset utilized input of manually segmented images, which can be time consuming and impractical. Future studies should

continue to take advantage of fully automated hematoma segmentation methods as they undergo validation.[29,30] As a promising preclinical study, our TBM model motivates additional external validation and prospective studies. These are needed to define its translation potential to a real-world clinical setting.

Conclusions

In this pre-clinical study, we present a quantitative and interpretable approach for discovery of non-contrast computed tomography (NCCT) markers of hematoma expansion in spontaneous intracerebral hemorrhage patients. Transport-based morphometry discriminated morphological characteristics of 24-hour hematoma expansion from presentation NCCT scans. Model inversion generated visual interpretations of the features discovered by the model. This quantitative approach has the potential to improve hematoma expansion prediction. Its interpretability informs mechanisms for hematoma expansion pathophysiology.

Materials and methods

Study Population

This analysis of spontaneous ICH patients was prepared according to the Standards for Reporting Diagnostic accuracy studies (STARD) guideline.[27] Subjects for model derivation were recruited from the Virtual International Trials in Stroke Archive (VISTA), which is an international multi-center collaborative pooled repository of anonymized patient data from randomized clinical trials.[27] Subjects for model external validation were recruited from the Ethnic/Racial Variations of Intracerebral Hemorrhage (ERICH) study, which is a multi-center, prospective, case-control study of ICH with emphasis on recruitment of .balanced proportions of non-Hispanic white, non-

Hispanic black and Hispanic ICH cases.[31] Inclusion criteria were: (1) age ≥18 years, (2) enrolment in neutral non-surgical ICH trials, (3) presentation with CT-proven ICH within 4 hours after symptom onset, (4) at least one subsequent CT scan at 24±6 hours after the initial scan, (5) available baseline clinical and laboratory data, (6) supratentorial location, and (7) initial volume ≥7 mL. Initial volume was set to distinguish microbleeds from the range of volumes associated with hematoma expansion.[32] Exclusion criteria were: (1) primary intraventricular hemorrhage (IVH), and (2) ICH related to suspected secondary causes. All required Institutional Review Board reviews and approval were completed at the respective institutions.

Clinical information

Clinical and demographic variables collected included age, sex, self-reported race/ethnicity, smoking at presentation (current or not current), previous ICH, anticoagulant use, presentation systolic blood pressure (mmHg), international normalized ratio, blood glucose (mg/dL), and time from symptom onset to first NCCT scan (min). To account for inter-patient differences in the time interval from symptom onset to presentation NCCT, hematoma growth rate was defined as: presentation hematoma volume divided by time from symptom onset to first NCCT (mL/min).

NCCT scan preprocessing

The de-identified NCCT scans at presentation and 24±6 hours after the initial scan were transferred in Digital Imaging and Communications in Medicine (DICOM) format to a central workstation. NCCT data was pre-processed according to a standard protocol as follows: (1) 3D DICOM CT images and their corresponding segmented hematoma regions were converted to a 3-channel NumPy array; (2) windowing was performed by applying a threshold of 0 to 150

Hounsfield Units (HU) to the original gray-scale NCCT image; (3) the region corresponding to skull was removed using the Brain Extraction Tool from the open source FMRIB Software Library version 6.0 (Analysis Group, FMRIB, Oxford, UK); (4) each NCCT image and its corresponding segmented hematoma region were registered to a population-based, high-resolution NCCT template and re-sized to dimensions of 256 x 256 x 256 with voxel spacings of 1 x 1 x 1mm using the Symmetric Normalization method from the Advanced Normalization Tools in Python package version 0.1.8; (5) the background of each NCCT image and its corresponding segmented hematoma region were cropped, reducing the image dimensions to 150 x 190 x 120; (6) segmented hematoma images located in the left hemisphere were translated across midline, so that all hematomas were registered in the right hemisphere; (7) a 3D curvature-driven gaussian filter with a step size of 0.125 using a total of 5 steps was applied to smooth the segmented hematoma images; (8) each segmented hematoma image was normalized so that the sum of its intensities was equal to 1. This protocol was intended to remove differences in CT acquisition methods to permit quantitative comparisons of segmented hematoma images. All pre-processed images were visually inspected (N.I., neurosurgeon in-training) evaluate for skull-stripping and registration errors prior to further analysis.

Hematoma segmentation

In the derivation dataset, hematoma regions were segmented by two independent raters who were blinded to outcomes information (T.R., board-certified neuroradiologist with 20 years of experience; K.E.N., neurosurgeon in-training), according to our previously described manual method.[30] Segmentations were adjudicated by a third rater (H.S., neurosurgeon in-training) and efforts were made to achieve a consensus in cases of significant inter-rater differences. In brief,

the ICH hyperdensity was traced on each two-dimensional (2D) slice of the 3D DICOM image stack, using the open-source software platform 3D Slicer version 4.10.2 (National Institutes of Health, Bethesda, MD). Visual inspection, with comparison to the contralateral hemisphere, was used to differentiate ICH from IVH, subdural and/or subarachnoid hemorrhage. In the external validation dataset, hematoma segmentation was performed according to our previously described fully automated convolutional neural network method.[30] In brief, the CNN architecture consisted of 31 convolutional and 7 pooling layers with a contracting and expanding topology. The rectified linear unit was used for all nonlinear functions. 50% dropout and L2 regularization were used to prevent overfitting.

Hematoma volumetry

After NCCT scan preprocessing, ICH volumes at presentation and 24±6 hours were measured by multiplying the number of voxels (volumetric pixels) in the segmented hematoma region by the volume of each voxel (1x1x1 mm).

3D transport-based morphometry

The optimal mass transport problem seeks the most efficient way of transforming one distribution of mass to another, by minimizing a cost function.[33] Transport-based morphometry (TBM) performs nonlinear image transformations by solving the continuous linear optimal transportation problem. Transforming images from their native domain to a transport domain affords three key advantages: (1) it permits discovery of discriminating image features that are not readily perceptible to the human eye, (2) it provides a physically meaningful metric, the Wasserstein distance, to quantify the relative changes in intensity between two images, and (3)

it interpolates between images to generate visual interpretations of the discriminating features discovered by the model.

Continuous linear optimal transport

We considered normalized Hounsfield Unit (HU) pixel intensity values as relative measurements of blood density and assumed that hematoma expansion occurs as a continuous process of red blood cell movement under the effect of unknown biological and physical influences.[14] This assumption allowed us to quantify the relative movement of blood density from one image to another. Normalizing each image so that the pixel intensities sum to the same total mass allows the images to be interpreted as probability measures. In this context, mass is represented as the image intensity.[34]

We consider two images I_0 and I_1 defined over their respective domains $\Omega_0$and Ω_1. Let I_1 represent an image of a segmented hematoma and I_0 represent the template image. Let MP refer to the set of mass preserving functions $f: \Omega_0 \to \Omega_1$ that rearranges the intensity co-ordinates of image I_0 to I_1. In other words: $MP := \{ f \mid det\,(D_f(\boldsymbol{x}))\, I_1(f(\boldsymbol{x})) = I_0(x)\,, det\,(D_f(\boldsymbol{x})) \geq 0 \forall \boldsymbol{x} \in \Omega_0\}$, with $D_f(\boldsymbol{x})$ representing the Jacobian matrix of deformation f computed at location x. The optimal mass transport function that rearranges the intensities of the two images can be computed by solving the minimization problem:

$$(1)\ \inf_{f \in M\ P} \int_{[0,1]^3} (f(\boldsymbol{x}) - \boldsymbol{x})^2 I_0(\boldsymbol{x}) d\boldsymbol{x}\ = W_2^2(I_0, I_1)$$

The minimizer of the optimal transport problem stated above is known as the squared

Wasserstein distance between the densities (images) I_0 and I_1, denoted above as $W_2^2(I_0, I_1)$. We utilize the previously described discretization and optimization approach to solve the optimal transport map between two digital images.[7,24]

The Linear Optimal Transport (LOT) framework takes I_0 to be a fixed reference image.[34,35] Given an image dataset $I_1, I_2, \cdots, I_k$, it calculates an embedding for image I_k by solving for the optimal mass rearrangement problem stated above between I_k and reference I_0. Note that given an optimal transport map f_k, and with knowledge of the fixed reference I_0, the image I_k can be recovered by computing (numerically) the inverse of the function (denoted as f^{-1}) and computing $\det\left(D_{f^{-1}}(x)\right) I_0\left(f^{-1}(x)\right) = I_1(y)$. For this reason, we can consider f_k to be a new invertible representation (transform) for image I_k. We use the notation $\widehat{I_k} = f_k$ to denote $\widehat{I_k}$ the LOT transform of I_k. The LOT representation (feature space) is then used to perform statistical analysis using standard techniques such as principal component analysis (PCA), linear discriminant analysis (LDA), and canonical correlation analysis (CCA). Specifically, analyses performed in LOT transform space utilize the so-called LOT distance:

$$(2)\quad D_{LOT}^2\left(I_k, I_j\right) = \| \widehat{I_k} - \widehat{I_j} \|^2 = \int_{\Omega_0} \left|\widehat{I_k}(\boldsymbol{x}) - \widehat{I_j}(\boldsymbol{x})\right|^2 d\boldsymbol{x}$$

Template image

The linear embedding is calculated with respect to an intrinsic mean template image I_0. The intrinsic mean template image I_0 represents the average hematoma appearance for the dataset. To estimate a reference given a set of images $I_1 \ldots I_N$, the Euclidean mean image is first computed according to:

$$\mu = 1/\mathrm{N}\sum_{\mathrm{i}=1}^{\mathrm{N}} \mathrm{I_k}$$

The set of mass preserving mappings that transform each image $\mathrm{I_k}$ into μ are computed using the minimization procedure described in equation (1). The mass preserving mappings f_k for $i = 1 \ldots N$ are then averaged:

$$f(\boldsymbol{x}) = 1/\mathrm{N}\sum_{\mathrm{i}=1}^{\mathrm{N}} f_k(\boldsymbol{x})$$

and used to iteratively update the Euclidean mean template image $\mathrm{I_0}$, according to:

$$I_0(x) = \det\big(D_f(x)\big)\,\mu(f(x))$$

The image $\mathrm{I_0}$ is then used as the reference for the LOT calculations described above.

Model derivation

Solving the continuous optimal transportation problem results in a unique linearly embedded 3D mass preserving (MP) map. We obtained the MP map for the segmented presentation NCCT hematoma image of each patient. In the derivation cohort, these data were shuffled at random and separated into independent training (60%) and internal validation (40%) cohorts for model derivation and optimization. To minimize bias in data sampling, this process was repeated 1000 times to generate 1000 different training and internal validation splits. The dataset composition is described further in the **Online-only supplement**. The code used for model derivation is available as an open-source package.[36]

Outcomes

Outcomes were (1) significant hematoma expansion, defined as ≥6mL increase in hematoma volume between the presentation and 24±6-hour NCCT scans, and (2) hematoma growth, defined as absolute hematoma volume (mL) increase between the presentation and 24±6 hour NCCT scans. Absolute hematoma volume increase (mL) was chosen for its reduced susceptibility to the effect of the size of the initial hematoma and stronger association with clinical outcome, than relative volume change (%). Significant hematoma expansion was set at 6 mL to reflect the threshold most used by established hematoma expansion prediction methods and in ICH clinical outcomes studies.[3,5,37] For the prediction of neurological outcome, lower hematoma expansion thresholds have been found to provide improved sensitivity at the expense of specificity, while higher thresholds provide improved specificity at the expense of sensitivity.[3,38]

Principal components analysis

Because the dimensionality of the hematoma image features in transport space was much higher than the number of data samples, we utilized the principal components analysis (PCA) for dimensionality reduction.[7,34] PCA is described in detail in the **Online-only supplement**. We retained the top *n* directions that explained 95% of the variance in the data. This eliminated the components with little contribution to the overall variance, reduced the likelihood of overfitting, and maintained separation of the training, internal validation and test datasets.

NCCT features discriminating hematoma expansion

To assess the relationship between presentation NCCT hematoma image features and 24-hour hematoma expansion, we used the penalized linear discriminant analysis (pLDA) method.[24]

Penalized Linear Discriminant Analysis (PLDA) is a modification of the Fisher linear discriminant analysis, described for morphometric studies of living tissues.[14] This is described in detail in the **Online-only supplement.**

We dichotomized patients into expansion and no expansion groups by the definition of ≥6mL and <6mL increase in hematoma volume from the presentation to the 24-hour NCCT scan.[3,5,37] We retained the top pLDA direction w^0 that maximally separated the two groups to train a classifier to assign patients to the expansion or no expansion groups. The reduced dimensionality matrix of the internal validation dataset, X_{test} was then projected onto w^o such that $Xw_{test} \in \mathbb{R}^{w^0 \times N_{test}}$. The independent t-test was used to assess the degree of separation between the histogram means of the expansion and no expansion groups in Xw_{test} and area under the receiver operator characteristic curve (AUROC) analyses evaluated the model's performance. Classification accuracy was assessed using sensitivity, specificity, positive predictive value (PPV) and negative predictive value (NPV).

Relationship between NCCT features and 24-hour hematoma volume change

The canonical correlation analysis (CCA) method determined the relationship between presentation NCCT hematoma image features and 24-hour change in hematoma volume (mL)[7,34] This is described in detail in the **Online-only supplement**. We retained the direction w_{corr} that was most correlated with change in hematoma volume (mL) between the presentation and 24±6 hour NCCT scans. The reduced dimensionality matrix of the internal validation dataset, X_{test} was then projected onto w_{corr} such that $Xw_{test} \in \mathbb{R}^{w_{corr} \times N_{test}}$. The Pearson's correlation coefficient (CC) was used to assess the strength of the relationship between Xw_{test} and 24-hour

hematoma volume change (mL).

Effect of location on expansion

To evaluate the independent effect of hematoma location on expansion, we defined location as the *x*, *y* and *z* co-ordinates of the center of each presentation NCCT hematoma image and used covariance matrices to represent the initial hematoma location with reference to the center of the mass of the template image $I_{0\mu}$. The abovementioned pLDA method and its corresponding statistical analyses were used to assess the effect of location for discriminating hematoma expansion.

Model optimization

We hypothesized that including location and clinical information would improve the model's overall performance. To test this, we rendered the MP maps location invariant by translating each presentation NCCT hematoma image according to its initial location with reference to the center of the mass of the template image $I_{0\mu}$. We compared baseline demographic and clinical information between expansion and no expansion groups using the χ^2, independent t- or non-parametric tests, as appropriate. To generate multivariable TBM models for predicting 24-hour hematoma expansion and hematoma growth, the x, y and z co-ordinates of the translation distances (mm) and the clinical variables for I_k represented as vectors $v = [v_1 \dots v_N]^T$, were concatenated with the principal components w_k of the derivation dataset X_{train} and X_{test}, such that $a_k = [w_k | v]$. Included clinical variables were age, sex, INR at presentation, and IVH score. The resultant multivariable training and internal validation matrices are given as $aX_{train} \in \mathbb{R}^{a_k \times N_{train}}$ and $aX_{test} \in \mathbb{R}^{a_k \times N_{test}}$, respectively. Their performance for discriminating

hematoma expansion and predicting future hematoma volume was assessed using abovementioned PLDA and CCA methods and their corresponding statistical analyses to obtain our final model.

External validation

An equivalent-sized dataset of 170 patients with a hematoma expansion rate of 25 – 33% was estimated to have a power of 0.97 – 0.99 to detect an AUC of 0.7 at the 0.05 significance level, given a null AUC of 0.5. For external validation of the model, we randomly sampled eligible patients from the ERICH repository to generate a test dataset of 170 patients with a equivalent number of hematoma expansion cases as the derivation dataset (n=56). In the test dataset, we obtained the MP map for the segmented presentation NCCT hematoma of each patient according to abovementioned methods. We performed dimensionality reduction using the abovementioned PCA method and adjusted for the relevant co-variates as determined by the optimal multivariable TBM model. The trained PLDA and CCA classifiers from the derivation dataset were applied to the external validation dataset and the optimal TBM model's performance for discriminating hematoma expansion and predicting future hematoma volume was assessed in the test dataset using abovementioned statistical analyses.

Visualization

The continuous linear optimal transportation approach is generative and any point in the transport space can be visualized by inverting its linear embedding. A synthetic image can be obtained from a displacement field v by first computing $\mathrm{f_v(x)} = \mathrm{x} - \mathrm{v(x)}$ with the following equation:

$$\det\left(D_{f_v^{-1}}(x)\right) I_0\left(f_v^{-1}(x)\right) = I_v(y)$$

where f_v^{-1} denotes the inverse of the mass-preserving optimal transport map.

We inverted the projections of the derivation dataset onto the principal pLDA direction w^0 to visualize the presentation NCCT hematoma image features discriminating hematoma expansion at 24 hours according to:

$$w_{pLDA} = \overline{X}_{train} + \sigma w^0$$

We also inverted the projections of the derivation dataset onto the most correlated CCA direction w_{corr} to visualize the presentation NCCT hematoma image features predicting greater hematoma volume increase at 24 hours according to:

$$w_{CCA} = \overline{X}_{train} + \sigma w_{corr}$$

where w_{pLDA} represented the direction and magnitude by which hematoma features differed between the expansion and no expansion groups, w_{CCA} represents the direction and magnitude by which hematoma image features were distributed according to changes in volume, $\overline{X}_{train}$ represents the center of $X_{train}$and σ is a length that has units of standard deviations of the projected data along w^0or w_{corr}.

To visualize the effect of hematoma location on expansion, we translated the inverse transformations of the location model according to w^o to visualize the *x*, *y* and *z* directions that discriminated hematoma expansion.

Hematoma morphometric feature detection

We visually interpreted the inverse transformations to identify the NCCT features of hematoma expansion discovered by the 3D-TBM model. To objectively assess the significance of these TBM-generated NCCT features of hematoma expansion, they were quantified from the presentation NCCT hematoma image data in its native domain. For each subject in the derivation dataset, we measured hematoma volume, density heterogeneity, shape eccentricity and density distribution, as described in detail in the **Online-only supplement**. For each NCCT feature, the independent *t*-test was used to assess the degree of separation achieved between the expansion and no expansion groups and AUROC analyses evaluated their predictive performance with comparison to the TBM model.

Comparison to alternate NCCT clinician-based prediction scores

Established NCCT features identified by clinicians to be associated with hematoma expansion were ranked by two independent trained raters who were blinded to outcomes information (A.B-G, neurosurgeon in-training; K.E.N., neurosurgeon in-training), as described in the **Online-only supplement**. These features were used in combination with clinical information to compute the existing BAT, BRAIN, HEAVN, NAG, hematoma expansion prediction, and 10-point clinical hematoma expansion prediction scores in each of the derivation and test datasets.[16,20-23] The performance of the TBM model in predicting 24-hour expansion with

comparison to each clinician-based score was assessed by AUROC analyses in the external validation dataset.

Comparison to alternate machine and deep learning methods

We trained classical machine learning models previously described for NCCT-based classification of hematoma expansion including support vector machine, logistic regression and k-nearest neighbors in the training dataset. We used PCA for dimensionality reduction prior to applying each classifier to the native presentation NCCT images.[39,40] ResNet is an emerging deep learning alternative for automated prediction of hematoma expansion.[41-43] We trained a 3D implementation of ResNet convolutional neural networks to classify hematoma expansion in the derivation dataset. The performance of the TBM model in predicting 24-hour expansion with comparison to each machine and deep learning method was assessed by AUROC analyses in the test dataset.

Statistical analyses

In the derivation dataset, statistical analyses and data visualization were performed independently on each of the 1000 cross-validation samples, and the mean results with corresponding 95% confidence intervals were obtained. Statistical analyses were performed using Stata 15.0 and Matlab R2022a. The *p*-values were averaged using the Fisher's method.[44] For both derivation and test datasets, statistical significance was defined as $p<0.05$.

Data availability

Data used for his manuscript is available from the corresponding author upon reasonable request.

Figure Legends

Figure 1. Example of the preprocessing protocol. **(A)** All NCCT scans were skull stripped and registered to a population-based high resolution NCCT template with dimensions of 256 x 256 x 256 and voxel spacings of 1 x 1 x 1mm. **(B)** example of a registered NCCT axial slice at presentation and **(C)** 24 hours in a patient with hematoma expansion. **(F)** the corresponding segmented and normalized hematoma image at presentation **(G)** and 24-hours for the same patient. **(D)** example of a registered NCCT axial slice at presentation **(E)** and 24 hours in a patient without hematoma expansion. **(H)** The corresponding normalized hematoma image at presentation **(I)** and 24-hours in the same patient. Examples of segmented presentation non-contrast computed tomography (NCCT) hematoma images separated into groups of **(J)** hematoma expansion (≥ 6mL hematoma volume increase at the 24 hour interval NCCT scan) and **(K)** no hematoma expansion (<6mL hematoma volume increase at the 24 hour interval NCCT scan), demonstrating a lack of visually discernible difference between the two groups. Abbreviations: NCCT = non-contrast computed tomography.

Figure 2. Results of the TBM model adjusted for location and clinical information in predicting 24-hour hematoma volume from the test dataset. **(A)** Scatter plots showing the relationship between the hematoma image features in the test dataset projected onto the most correlated direction w_{corr} in transport space and change in hematoma volume from the presentation to the 24-hour NCCT scan. **(B)** Inverse transformations of three two-dimensional axial slice examples of the hematoma morphometric features found by the model to be associated with increasing growth, shown from left to right of the *x*-axis **(C)** Inverse transformations of the hematoma morphometric features overlaid onto the axial NCCT scan associated with *least* growth, left, and *most* growth, right. Abbreviations: NCCT = non-contrast computed tomography, TBM = transport-based morphometry, CC = correlation co-efficient σ = standard deviation of the pixel intensity distribution along w_{corr}.

Figure 3. Results of the TBM model adjusted for location and clinical information in predicting 24-hour hematoma expansion from the test dataset. **(A)** Mean probability distributions of the hematoma image features in the test dataset projected onto the most discriminant direction w_0 in transport space showing the degree of separation between the expansion (red) and no expansion (blue) groups by the learned pLDA classifier boundary. **(B)** AUROC analyses and corresponding 95% confidence intervals of the performance of the pLDA classifier in the test dataset for **(C)** Inverse transformations of three two-dimensional axial slice examples of the hematoma morphometric features found by the model to be associated with increasing likelihood of expansion, shown from left to right of the *x*-axis **(D)** Inverse transformations of the hematoma morphometric features overlaid onto the axial NCCT scan *least* associated with expansion, left, and *most* associated with expansion, right. Abbreviations: NCCT = non-contrast computed tomography, TBM = transport-based morphometry, AUROC = area under the receiver operator curve, pLDA = penalized linear discriminant analysis, σ = standard deviation of the pixel intensity distribution along w_0.

Figure 4. Independent effects of hematoma location as a predictor of 24-hour hematoma expansion. Two-dimensional examples of inverse transformations overlaid onto NCCT scans in the axial (top row), sagittal (second row) and coronal (third row) planes showing from left to right of the *x*-axis the hematoma morphometric features and location direction found by the TBM model to be associated with increasing likelihood of expansion. Abbreviations: NCCT = non-contrast computed tomography, TBM = transport-based morphometry, σ = standard deviation of the pixel intensity distribution along w_0.

Figure 5: Comparisons of the performance of existing NCCT hematoma expansion prediction scores with comparison to the final TBM model adjusted for location and clinical information in test dataset. Hematoma expansion was defined as ≥ 6mL hematoma volume increase from the presentation to the 24±6 hour NCCT scan. Abbreviations: AUROC = Area Under the Receiver Operator Curve, ROC = Receiver Operator Curve, TBM = transport-based morphometry, NCCT = non-contrast computed tomography, HEAVN = Heavn score, Brain = Brain score, HEP = Hematoma expansion prediction score, Pt = 10-point score, BAT = BAT score, TBM =

transport-based morphometry.

References

1. Rzepliński R, Sługocki M, Tarka S, et al. Mechanism of spontaneous intracerebral hemorrhage formation: an anatomical specimens-based study. *Stroke*. 2022;53(11):3474-3480.
2. Fisher CM. Pathological observations in hypertensive cerebral hemorrhage. *J Neuropathol Exp Neurol*. Jul 1971;30(3):536-50. doi:10.1097/00005072-197107000-00015
3. Mayer SA, Frontera JA, Jankowitz B, et al. Recommended Primary Outcomes for Clinical Trials Evaluating Hemostatic Agents in Patients With Intracranial Hemorrhage: A Consensus Statement. *JAMA Netw Open*. Sep 1 2021;4(9):e2123629. doi:10.1001/jamanetworkopen.2021.23629
4. Naidech AM, Grotta J, Elm J, et al. Recombinant factor VIIa for hemorrhagic stroke treatment at earliest possible time (FASTEST): Protocol for a phase III, double-blind, randomized, placebo-controlled trial. *Int J Stroke*. Aug 2022;17(7):806-809. doi:10.1177/17474930211042700
5. Yogendrakumar V, Moores M, Sikora L, et al. Evaluating Hematoma Expansion Scores in Acute Spontaneous Intracerebral Hemorrhage: A Systematic Scoping Review. *Stroke*. Apr 2020;51(4):1305-1308. doi:10.1161/strokeaha.119.028574
6. Wang F, Casalino LP, Khullar D. Deep learning in medicine—promise, progress, and challenges. *JAMA internal medicine*. 2019;179(3):293-294.
7. Kundu S, Kolouri S, Erickson KI, Kramer AF, McAuley E, Rohde GK. Discovery and visualization of structural biomarkers from MRI using transport-based morphometry. *NeuroImage*. 2018;167:256-275.
8. Kundu S, Ashinsky BG, Bouhrara M, et al. Enabling early detection of osteoarthritis from presymptomatic cartilage texture maps via transport-based learning. *Proc Natl Acad Sci U S A*. Oct 6 2020;117(40):24709-24719. doi:10.1073/pnas.1917405117
9. Kolouri S, Park S, Thorpe M, Slepčev D, Rohde GK. Optimal Mass Transport: Signal processing and machine-learning applications. *IEEE Signal Process Mag*. Jul 2017;34(4):43-59. doi:10.1109/msp.2017.2695801
10. Huttner HB, Gerner ST, Kuramatsu JB, et al. Hematoma Expansion and Clinical Outcomes in Patients With Factor-Xa Inhibitor-Related Atraumatic Intracerebral Hemorrhage Treated Within the ANNEXA-4 Trial Versus Real-World Usual Care. *Stroke*. Feb 2022;53(2):532-543. doi:10.1161/strokeaha.121.034572
11. Morotti A, Boulouis G, Charidimou A, et al. Hematoma Expansion in Intracerebral Hemorrhage With Unclear Onset. *Neurology*. May 11 2021;96(19):e2363-e2371. doi:10.1212/wnl.0000000000011895
12. Brott T, Broderick J, Kothari R, et al. Early hemorrhage growth in patients with intracerebral hemorrhage. *Stroke*. Jan 1997;28(1):1-5. doi:10.1161/01.str.28.1.1
13. Brouwers HB, Greenberg SM. Hematoma expansion following acute intracerebral hemorrhage. *Cerebrovasc Dis*. 2013;35(3):195-201. doi:10.1159/000346599
14. Basu S, Kolouri S, Rohde GK. Detecting and visualizing cell phenotype differences from microscopy images using transport-based morphometry. *Proc Natl Acad Sci U S A*. Mar 4 2014;111(9):3448-53. doi:10.1073/pnas.1319779111
15. Hemphill JC, 3rd. Hematoma Expansion in ICH: Targeting Epidemiology or Biology? *Neurocrit Care*. Aug 2019;31(1):9-10. doi:10.1007/s12028-019-00752-1
16. Morotti A, Dowlatshahi D, Boulouis G, et al. Predicting Intracerebral Hemorrhage Expansion With Noncontrast Computed Tomography: The BAT Score. *Stroke*. May 2018;49(5):1163-1169. doi:10.1161/strokeaha.117.020138
17. Morotti A, Boulouis G, Dowlatshahi D, et al. Standards for Detecting, Interpreting, and Reporting Noncontrast Computed Tomographic Markers of Intracerebral Hemorrhage Expansion. *Ann Neurol*. Oct 2019;86(4):480-492. doi:10.1002/ana.25563
18. Morotti A, Arba F, Boulouis G, Charidimou A. Noncontrast CT markers of intracerebral hemorrhage expansion and poor outcome: A meta-analysis. *Neurology*. Oct 6 2020;95(14):632-643. doi:10.1212/wnl.0000000000010660
19. Lv XN, Deng L, Yang WS, Wei X, Li Q. Computed Tomography Imaging Predictors of Intracerebral Hemorrhage Expansion. *Curr Neurol Neurosci Rep*. Mar 12 2021;21(5):22. doi:10.1007/s11910-021-01108-z
20. Wang X, Arima H, Al-Shahi Salman R, et al. Clinical prediction algorithm (BRAIN) to determine risk of hematoma growth in acute intracerebral hemorrhage. *Stroke*. Feb 2015;46(2):376-81. doi:10.1161/strokeaha.114.006910
21. Miyahara M, Noda R, Yamaguchi S, et al. New Prediction Score for Hematoma Expansion and Neurological Deterioration after Spontaneous Intracerebral Hemorrhage: A Hospital-Based Retrospective Cohort Study. *J Stroke Cerebrovasc Dis*. Sep 2018;27(9):2543-2550. doi:10.1016/j.jstrokecerebrovasdis.2018.05.018

22. Sakuta K, Sato T, Komatsu T, et al. The NAG scale: Noble Predictive Scale for Hematoma Expansion in Intracerebral Hemorrhage. *J Stroke Cerebrovasc Dis*. Oct 2018;27(10):2606-2612. doi:10.1016/j.jstrokecerebrovasdis.2018.05.020
23. Fu J, Hu S, Yang M, et al. A Novel 10-Point Score System to Predict Early Hematoma Growth in Patients With Spontaneous Intracerebral Hemorrhage. *Front Neurol*. 2019;10:1417. doi:10.3389/fneur.2019.01417
24. Kolouri S, Tosun AB, Ozolek JA, Rohde GK. A continuous linear optimal transport approach for pattern analysis in image datasets. *Pattern Recognit*. Mar 1 2016;51:453-462. doi:10.1016/j.patcog.2015.09.019
25. Vagal A, Wintermark M, Nael K, et al. Automated CT perfusion imaging for acute ischemic stroke: Pearls and pitfalls for real-world use. *Neurology*. Nov 12 2019;93(20):888-898. doi:10.1212/wnl.0000000000008481
26. Automated CT Perfusion Imaging to Aid in the Selection of Patients With Acute Ischemic Stroke for Mechanical Thrombectomy: A Health Technology Assessment. *Ont Health Technol Assess Ser*. 2020;20(13):1-87.
27. Ali M, Bath P, Brady M, et al. Development, expansion, and use of a stroke clinical trials resource for novel exploratory analyses. *Int J Stroke*. Feb 2012;7(2):133-8. doi:10.1111/j.1747-4949.2011.00735.x
28. Miller MM, Rubaiyat AHM, Rohde GK. Predicting Malignancy of Breast Imaging Findings Using Quantitative Analysis of Contrast-Enhanced Mammography (CEM). *Diagnostics (Basel)*. Mar 16 2023;13(6)doi:10.3390/diagnostics13061129
29. Ironside N, Patrie J, Ng S, et al. Quantification of hematoma and perihematomal edema volumes in intracerebral hemorrhage study: Design considerations in an artificial intelligence validation (QUANTUM) study. *Clinical Trials*. 2022;19(5):534-544.
30. Ironside N, Chen CJ, Mutasa S, et al. Fully Automated Segmentation Algorithm for Hematoma Volumetric Analysis in Spontaneous Intracerebral Hemorrhage. *Stroke*. Dec 2019;50(12):3416-3423. doi:10.1161/strokeaha.119.026561
31. Woo D, Rosand J, Kidwell C, et al. The Ethnic/Racial Variations of Intracerebral Hemorrhage (ERICH) study protocol. *Stroke*. Oct 2013;44(10):e120-5. doi:10.1161/strokeaha.113.002332
32. Al-Shahi Salman R, Frantzias J, Lee RJ, et al. Absolute risk and predictors of the growth of acute spontaneous intracerebral haemorrhage: a systematic review and meta-analysis of individual patient data. *Lancet Neurol*. Oct 2018;17(10):885-894. doi:10.1016/s1474-4422(18)30253-9
33. Monge G. Mémoire sur la théorie des déblais et des remblais. *Mem Math Phys Acad Royale Sci*. 1781:666-704.
34. Wang W, Slepčev D, Basu S, Ozolek JA, Rohde GK. A linear optimal transportation framework for quantifying and visualizing variations in sets of images. *Int J Comput Vis*. Jan 1 2013;101(2):254-269. doi:10.1007/s11263-012-0566-z
35. Aldroubi A, Li S, Rohde GK. Partitioning signal classes using transport transforms for data analysis and machine learning. *Sampling theory, signal processing, and data analysis*. 2021;19(1):6.
36. Rohde GK. PyTransKit. https://github.com/rohdelab/PyTransKit
37. Dowlatshahi D, Demchuk AM, Flaherty ML, Ali M, Lyden PL, Smith EE. Defining hematoma expansion in intracerebral hemorrhage: relationship with patient outcomes. *Neurology*. Apr 5 2011;76(14):1238-44. doi:10.1212/WNL.0b013e3182143317
38. Morotti A, Boulouis G, Dowlatshahi D, et al. Intracerebral haemorrhage expansion: definitions, predictors, and prevention. *Lancet Neurol*. Feb 2023;22(2):159-171. doi:10.1016/s1474-4422(22)00338-6
39. Swetz D, Seymour SE, Rava RA, et al. Initial investigation of predicting hematoma expansion for intracerebral hemorrhage using imaging biomarkers and machine learning. *Proc SPIE Int Soc Opt Eng*. Feb-Mar 2022;12036doi:10.1117/12.2610672
40. Tanioka S, Yago T, Tanaka K, et al. Machine learning prediction of hematoma expansion in acute intracerebral hemorrhage. *Sci Rep*. Jul 21 2022;12(1):12452. doi:10.1038/s41598-022-15400-6
41. Lu M, Wang Y, Tian J, Feng H. Application of deep learning and radiomics in the prediction of hematoma expansion in intracerebral hemorrhage: a fully automated hybrid approach. *Diagn Interv Radiol*. Apr 24 2024;doi:10.4274/dir.2024.222088
42. Ma C, Wang L, Gao C, et al. Automatic and Efficient Prediction of Hematoma Expansion in Patients with Hypertensive Intracerebral Hemorrhage Using Deep Learning Based on CT Images. *J Pers Med*. May 12 2022;12(5)doi:10.3390/jpm12050779
43. Lee H, Lee J, Jang J, et al. Predicting hematoma expansion in acute spontaneous intracerebral hemorrhage: integrating clinical factors with a multitask deep learning model for non-contrast head CT. *Neuroradiology*. Apr 2024;66(4):577-587. doi:10.1007/s00234-024-03298-y
44. Fisher RA. Statistical methods for research workers. 1936;

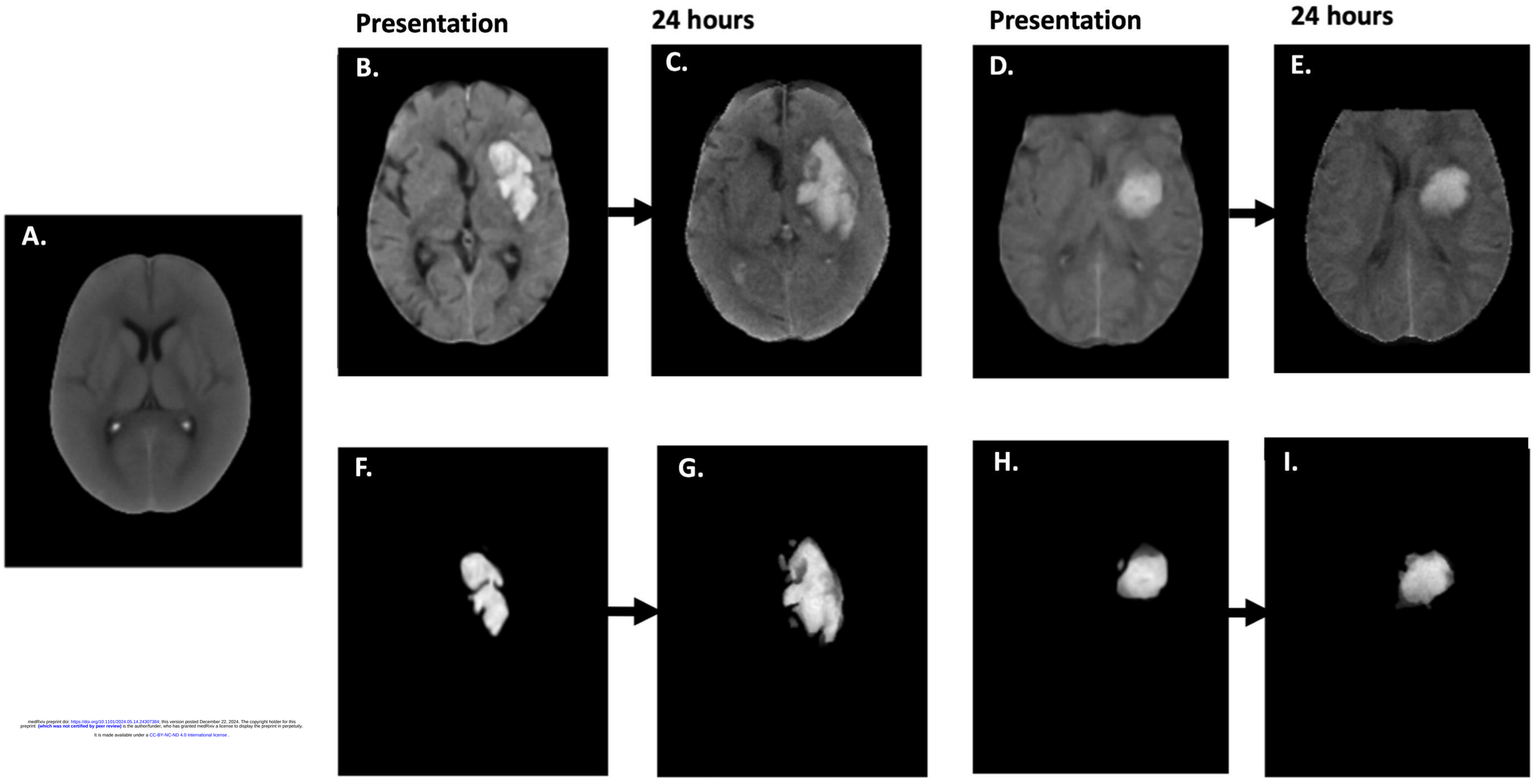

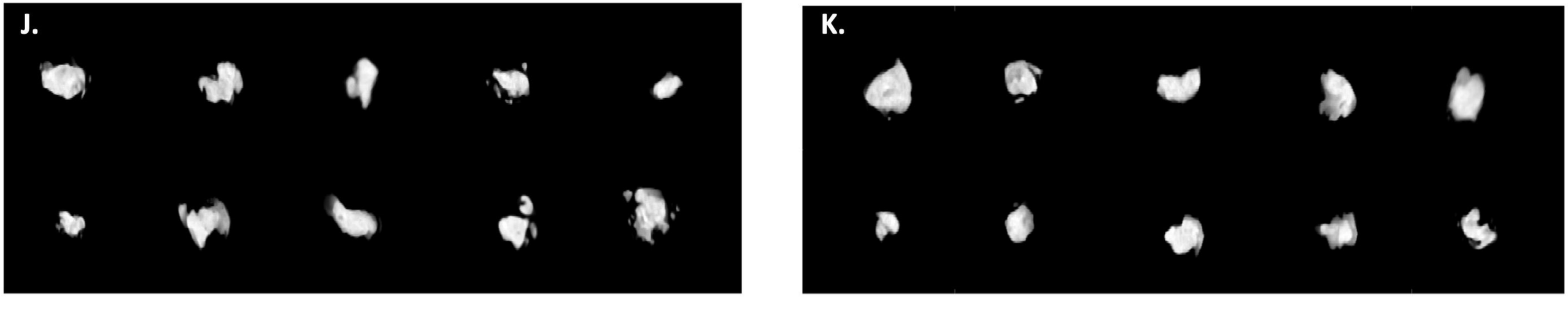

A.

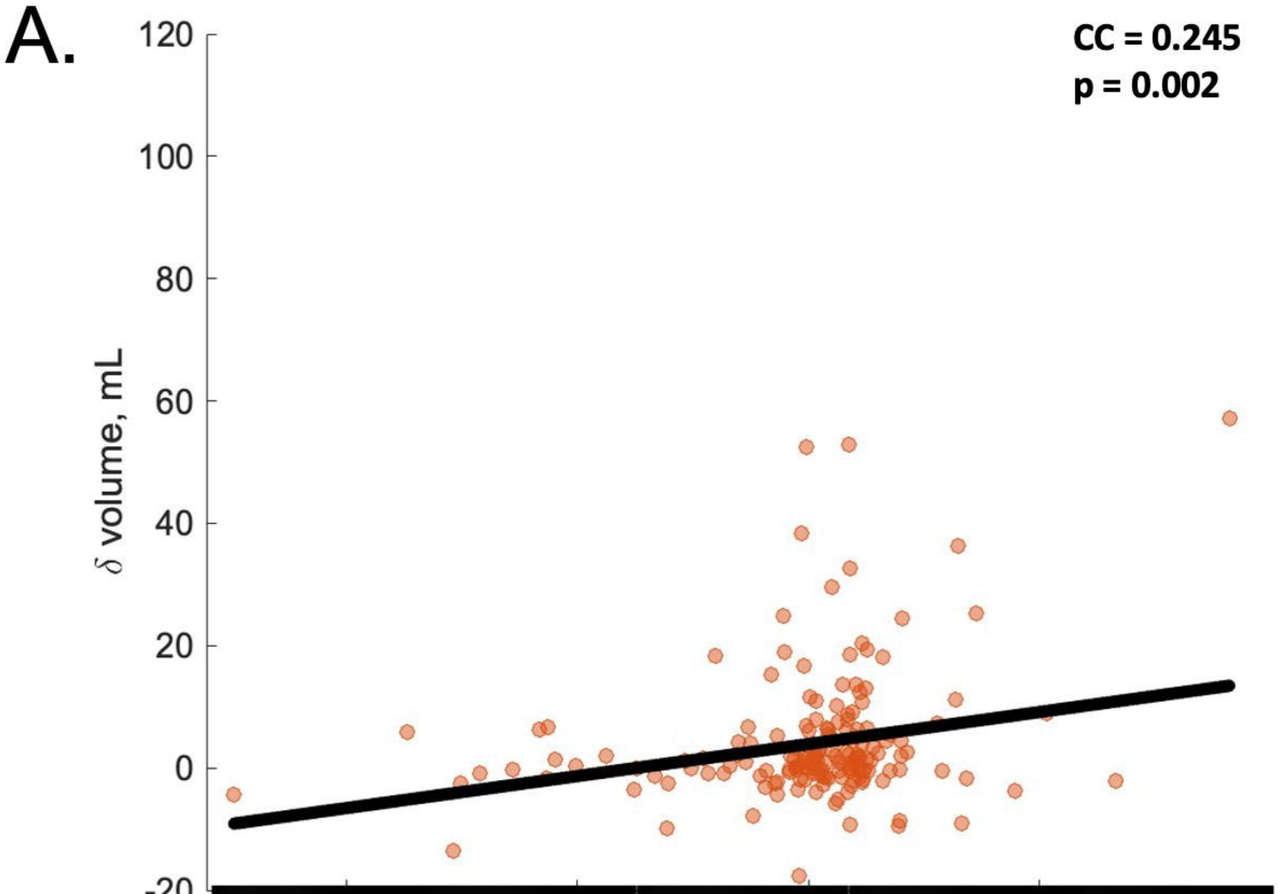

B.

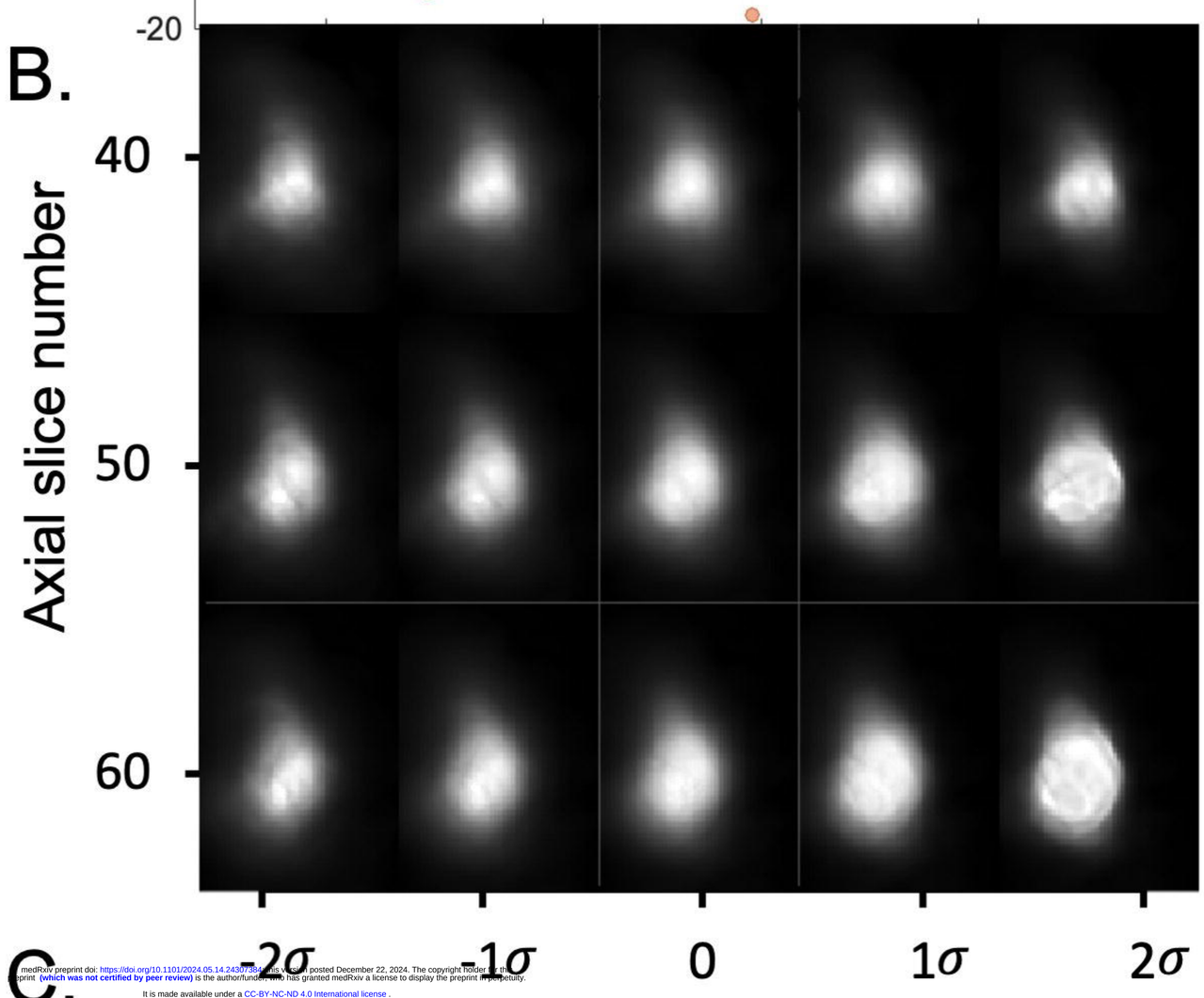

C.

A.

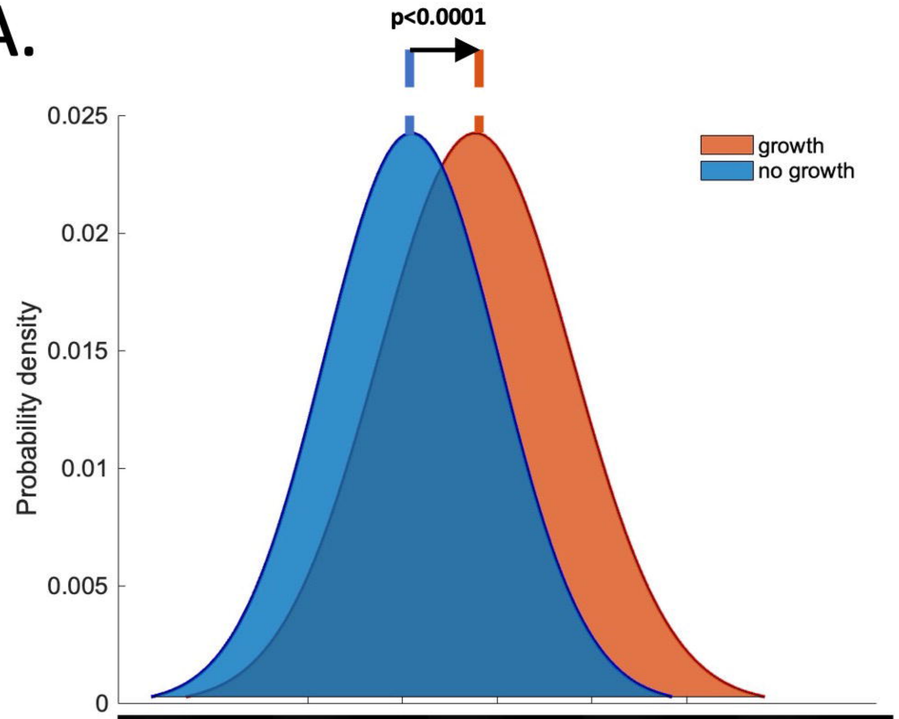

B.

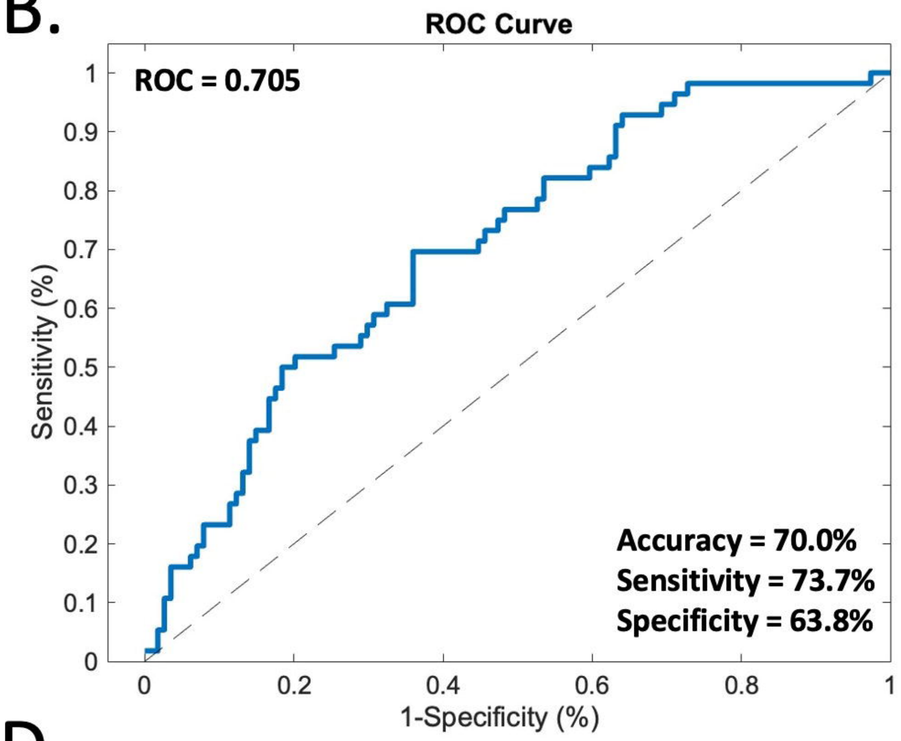

C.

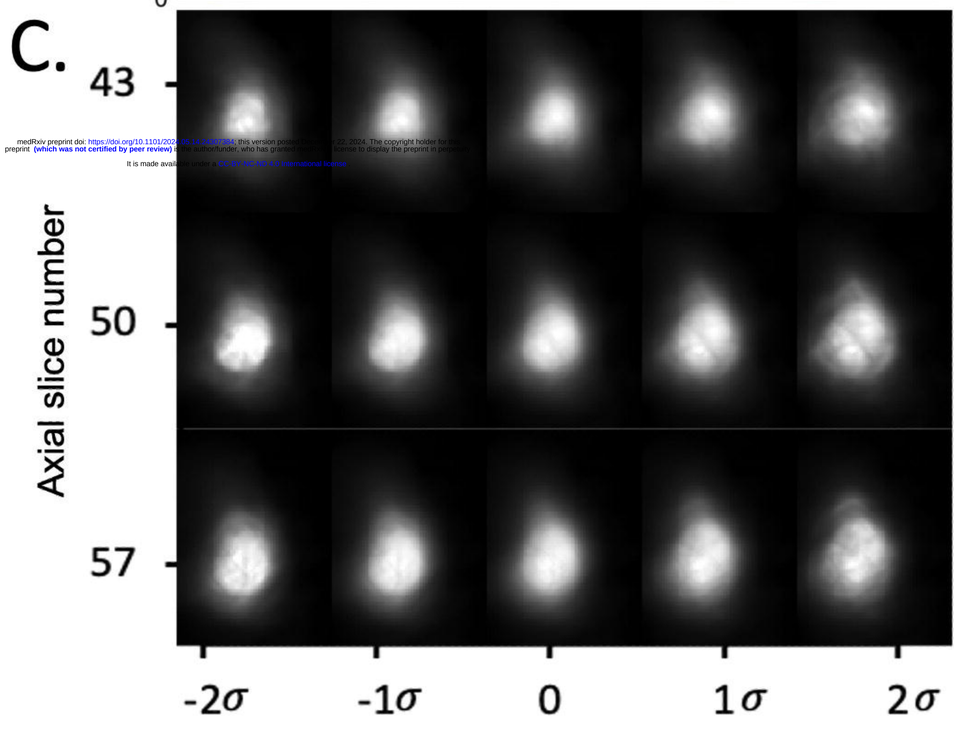

D.

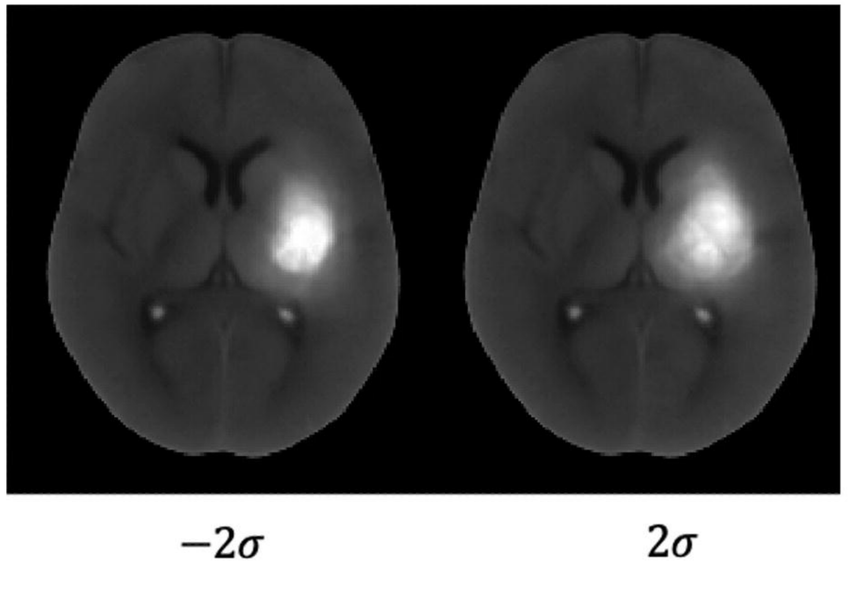

AUROC = 0.600 [0.597 – 0.603]